AD_____

AWARD NUMBER DAMD17-96-1-6265

TITLE: Structure and Inhibition of the neu-erbB-2 Receptor

PRINCIPAL INVESTIGATOR: David F. Stern, Ph.D.

CONTRACTING ORGANIZATION: Yale University
New Haven, Connecticut 06520-8047

REPORT DATE: September 1998

TYPE OF REPORT: Final

PREPARED FOR: Commanding General
U.S. Army Medical Research and Materiel Command
Fort Detrick, Maryland 21702-5012

# REPORT DOCUMENTATION PAGE

*Form Approved*
*OMB No. 0704-0188*



| 1. AGENCY USE ONLY *(Leave blank)* | 2. REPORT DATE | 3. REPORT TYPE AND DATES COVERED |
|---|---|---|
| | September 1998 | Final (1 Sep 96 - 31 Aug 98) |

**4. TITLE AND SUBTITLE**
Structure and Inhibition of the neu-erbB-2 Receptor

**5. FUNDING NUMBERS**
DAMD17-96-1-6265

**6. AUTHOR(S)**
David F. Stern, Ph.D.

**7. PERFORMING ORGANIZATION NAME(S) AND ADDRESS(ES)**
Yale University
New Haven, Connecticut 06520-8047

**8. PERFORMING ORGANIZATION REPORT NUMBER**

**9. SPONSORING / MONITORING AGENCY NAME(S) AND ADDRESS(ES)**
U.S. Army Medical Research and Materiel Command
Fort Detrick, Maryland 21702-5012

**10. SPONSORING / MONITORING AGENCY REPORT NUMBER**

**11. SUPPLEMENTARY NOTES**

19981221 012

**12a. DISTRIBUTION / AVAILABILITY STATEMENT**
Approved for Public Release; Distribution Unlimited

**12b. DISTRIBUTION CODE**

**13. ABSTRACT** *(Maximum 200 words)*

The *neu/erbB-2* gene encodes a 185 kD receptor tyrosine kinase which is constitutively activated by either gene overexpression or by a single mutation, valine to glutamic acid, at position 664 within its hydrophobic transmembrane domain. The goal of the research project has been to obtain the high resolution structure of the receptor transmembrane domain and to establish the mechanism by which the Glu664 mutation leads to receptor activation. Based on NMR-derived distance contraints, we have found that Glu664 drives dimerization of the transmembrane domain through hydrogen-bonding inteactions. Moreover, Gly665 and Ala661 pack in the dimer interface and stabilize the helix dimer through van der Waals interactions. The polar threonine residues at positions 662 and 657 also serve to stabilize the dimer through hydrogen bonding interactions. The observation of deuterium exchange of four engineered cysteines in the C-terminus of the transmembrane domain is consistent with a large helix crossing angle. Based on these studies we suggest that specific inhibitors to the activated neu sequence should target the polar threonine and glutamic acid residues, as well as the van der Waals surfaces created by Gly665 and Ala661, both of which have small side chains and allow good packing interactions.

| 14. SUBJECT TERMS | 15. NUMBER OF PAGES |
|---|---|
| Breast Cancer | 37 |
| | 16. PRICE CODE |

| 17. SECURITY CLASSIFICATION OF REPORT | 18. SECURITY CLASSIFICATION OF THIS PAGE | 19. SECURITY CLASSIFICATION OF ABSTRACT | 20. LIMITATION OF ABSTRACT |
|---|---|---|---|
| Unclassified | Unclassified | Unclassified | Unlimited |

## FOREWORD

Opinions, interpretations, conclusions and recommendations are those of the author and are not necessarily endorsed by the U.S. Army.

____ Where copyrighted material is quoted, permission has been obtained to use such material.

____ Where material from documents designated for limited distribution is quoted, permission has been obtained to use the material.

____ Citations of commercial organizations and trade names in this report do not constitute an official Department of Army endorsement or approval of the products or services of these organizations.

____ In conducting research using animals, the investigator(s) adhered to the "Guide for the Care and Use of Laboratory Animals," prepared by the Committee on Care and use of Laboratory Animals of the Institute of Laboratory Resources, national Research Council (NIH Publication No. 86-23, Revised 1985).

✓ For the protection of human subjects, the investigator(s) adhered to policies of applicable Federal Law 45 CFR 46.

____ In conducting research utilizing recombinant DNA technology, the investigator(s) adhered to current guidelines promulgated by the National Institutes of Health.

____ In the conduct of research utilizing recombinant DNA, the investigator(s) adhered to the NIH Guidelines for Research Involving Recombinant DNA Molecules.

____ In the conduct of research involving hazardous organisms, the investigator(s) adhered to the CDC-NIH Guide for Biosafety in Microbiological and Biomedical Laboratories.

9/25/98

PI - Signature Date

9/25/98

## TABLE OF CONTENTS

Structure and Inhibition of the neu/erbB-2 Receptor

## INTRODUCTION

The research undertaken here has been to study the structure of one critical membrane receptor, the neu or erbB-2 receptor, whose activation has been associated with a large number of breast and ovarian cancers. Generally, cancer results from a breakdown in the normal mechanisms which control the growth and division of cells. For many cells, the signals for initiating cell division are hormone molecules that bind to receptors on the surface of the cell. The signal is transmitted through the cell membrane by one or more receptor molecules. Receptors in an "active" state (with hormones bound) initiate a cascade of events which starts the replication machinery. Uncontrolled cell transformation often results when the receptors on the cell surface are "turned on" even in the absence of the signalling hormone.

The neu receptor normally signals by dimerizing in response to hormone binding. The *neu/erbB-2* gene encodes a 185 kD receptor tyrosine kinase and is part of the erbB family of receptor tyrosine kinases; it has two cysteine-rich extracellular domains, a single helical membrane-spanning domain and an intracellular tyrosine kinase (TK) domain. Constitutive activation of the receptor is known to occur by gene overexpression or by a single mutation within the hydrophobic transmembrane sequence where a naturally-occurring valine residue at position 664 is replaced by glutamic acid [1-4]. The point mutation was the first occurrence of an activating mutation in the transmembrane domain of a growth factor receptor and has suggested that the structure of the transmembrane domain plays a larger role in the signal transduction process than previously thought. The goal of the research project has been to obtain the *three dimensional structure* of the neu receptor transmembrane domain and to establish the *mechanism* by which the Glu 664 mutation leads to receptor activation.

Figure 1 shows a helical wheel diagrams of the neu (V664) and activated neu (E664) transmembrane domain. The sequences are largely hydrophobic. Of importance are the polar serine and threonine residues on the N-terminal side of position 664 and the glycine residue at position 665. Two models have been proposed for how the Val 664 -> Glu 664 substitution causes cell transformation. The first involves a change in the secondary structure of the transmembrane (TM) domain. Brandt-Rauf et al. (1990) [5] calculated that the minimum-energy conformation in the region of Val 664 contains a sharp bend at positions 664 and 665, while the transforming sequence exists as an $\alpha$-helix. The second model is that the glutamate side chain promotes dimerization via hydrogen-bonding interactions [6]. In this case, the helices are thought to be held in the "active" state by hydrogen bonding between the Glu 664 carboxylic acid side chain on one helix and the Glu 664 side chain or peptide backbone carbonyl and amide groups of the second helix. Consistent with this model, the transforming protein (with a glutamic acid residue at position, Glu 664) has a higher propensity to form dimers than the normal (Val 664) protein [7]. The position of the glutamic acid residue is sequence specific. Bargmann and Weinberg originally demonstrated that substitution of glutamic acid at positions 663 or 665 did not activate the receptor [1].

Stern and coworkers have undertaken an extensive mutagenesis study of the TM domain of *neu* to define the residues that are responsible for receptor activation [4]. They found that a sub-domain, $-V_{663}- E_{664} -G_{665}-$, is important. The domain differs slightly from that predicted by Sternberg and Gullick [6], most notably in the importance of $A_{661}$ for receptor dimerization. Gullick and coworkers [8] have shown that intracellular expression of small proteins, corresponding to the TM and membrane-proximal domains of neu and containing variations on the activated neu TM

sequence, inhibits growth of neu transformed cells. However, a simple model involving hydrogen-bonding interactions of the Glu 664 may not be sufficient to explain receptor activation. Stern and coworkers [4] have shown, by moving the VEG sub-domain around in the TM sequence and by generating mutants that dimerize without activating the receptor, that dimerization alone is insufficient to cause cell transformation and that the interactions are likely to be highly specific. No direct evidence has been obtained for the points of contact in the receptor dimers and a high-resolution structure is needed to determine the exact nature of the protein interactions and whether they are distributed along the length of the TM domain.

In order to determine the structure of the transmembrane domain of the neu/erbB-2 receptor and address the molecular mechanism of receptor activation by the transforming Val 664 to Glu 664 mutation, magic angle spinning (MAS) NMR and polarized Fourier transform infrared (FTIR) studies have been undertaken. We have previously shown that MAS NMR and FTIR measurements provide a feasible approach for structural studies on membrane proteins [9-11].

MAS yields high resolution NMR spectra of membrane proteins in bilayer environments [6] and several different strategies have been developed for measuring weak dipolar couplings in MAS experiments [12-15]. Of importance for structural studies is that accurate internuclear distances can be derived from measurements of dipolar couplings which in turn provide constraints for generating and evaluating structural models. The two best established approaches are rotational resonance (RR) and rotational echo double resonance (REDOR) NMR. The RR NMR approach selectively restores the dipolar couplings by spinning the sample such that an integral multiple of the MAS frequency is equal to the chemical shift difference ($\Delta\omega$) between two NMR resonances [16-18]. The distance limits for $^{13}C...^{13}C$ measurements using RR NMR is ~6.5 Å with resolution on the order of 0.3 Å. The REDOR NMR approach has been developed to measure weak heteronuclear dipolar couplings, such as those between $^{31}P$ and $^{13}C$ or $^{15}N$ and $^{13}C$ [19,20]. REDOR relies on the dephasing of magnetization of the observed spin through coupling to a second spin. The distance limit for $^{13}C...^{15}N$ measurements using REDOR NMR is ~5 Å with resolution on the order of 0.2 Å.

The global secondary structure and orientation of membrane proteins and peptides can be probed by polarized FTIR spectroscopy using the amide I vibration as a structurally sensitive marker [21]. The frequency of the amide I mode depends on hydrogen-bonding of the C=O group as well as on the geometry of the peptide backbone. Bands centered at ~1654 $cm^{-1}$ correspond to $\alpha$-helical structures, while bands centered at 1624 - 1637 $cm^{-1}$ and 1675 $cm^{-1}$ correspond to the out-of-phase and in-phase modes of $\beta$-sheet structures, respectively or alternatively $\beta$-turn. Fourier self deconvolution (FSD) of the amide I region [22] can yield quantitative estimates of the relative ratios between the different secondary structural elements of the protein [23]. The orientation of C=O group, which dominates the amide I vibration, can be derived from the relative absorption of IR light polarized parallel or perpendicular to the C=O transition dipole moment. Maximum absorption occurs when the polarization of light is parallel to the transition moment. In an $\alpha$-helix, the C=O transition dipole is known to be oriented at an angle of ~39° relative to the helix axis [24-26].

During the first year of this research project, considerable progress was made in obtaining high resolution structural constraints of the neu receptor transmembrane domain. We showed that the transmembrane domain forms a well-folded dimer of long helices oriented perpendicular to the membrane surface. Magic angle spinning NMR methods for measuring internuclear distances provided accurate distance constraints within and between transmembrane helices, while polarized

infrared measurements established one additional helix-helix contact in the transmembrane dimer at postion 661. Based on this data, computational searches generated low energy structures of the transmembrane dimer to evaluate and interpret the structural data.

During the last year of this project, additional NMR and IR measurements were undertaken to refine the structural model we have been developing. One of the critical question that we have been investigating has been the influence of the membrane environment on the association of the neu transmembrane domains. We originally measured a relative short internuclear distance between the side chain of a glutamine residue at position 664 in the sequence and its neighbor across the dimer interface. This indicated that the key glutamine residues were hydrogen bonding to one another in the dimer complex. However, the data indicated that the interactions were nonsymmetric. Recently, we have shown that the nonsymmetry resulted from heterogeneity in the sample which could be eliminated by changing the reconstitution protocol. Currently the best structural model for the dimer interface in the region of position 664 reveals that Gly 665 residues in the dimer interface and hydrogen bonding interactions of the Glu 664 side chains to polar threonine hydroxyl groups across the dimer interface. The helices are predicted to cross in a right-handed coiled coil geometry.

Finally, the research described in this report is primarily that of Dr. Steven Smith, the original principal investigator. Dr. Smith relocated his research group from Yale University to SUNY Stony Brook on July 1, 1998 and a request to transfer the grant to Dr. David Stern was approved.

## BODY

### Experimental Methods

*Synthesis of neuTM and neu*TM.* The neuTM and neu*TM peptides were synthesized using solid-phase methods at the Keck Peptide Synthesis Facility at Yale University. The sequence of the 38-residue peptides corresponds to residues 649-686 in the neu receptor protein. The sequence of neu*TM is shown below.

AEQRASPVTFIIATV-E664-GVLLFLALVVVVGILIKRRRYK

The lyophilized peptide was dissolved in trifluoroacetic acid and purified using a 5 ml POROS-R1 reverse phase high performance liquid chromatography (RP-HPLC) column (Perceptive Biosystems, Cambridge, MA) equilibrated with 95% $H_2O$, 2% acetonitrile and 3% 2-propanol. Peptide elution was achieved with a linear gradient to a final solvent composition of 5% $H_2O$, 38% acetonitrile and 57% 2-propanol. All solvents contained 0.1% trifluoroacetic acid. Fractions containing peptides were then lyophilized and assessed for purity by amino acid analysis (correlation coefficients of > 0.95) and mass spectrometry. Following lyophilization, peptides were reconstituted into membranes as described in *Procedures* below.

*Fourier Transform Infrared Spectroscopy.* FTIR spectra were recorded on a Nicolet Magna 550 spectrometer purged with $N_2$ (Madison, WI) and equipped with a MCT/A detector. For transmission spectra, typically 50 µl of sample (protein concentration of 36 - 90 mM) is dried on AgCl windows with dry air. For polarized ATR-FTIR spectra, the spectrometer was equipped with a KRS-5 wire grid polarizer (0.25 mm spacing, Grasbey Specac, Kent, UK). The sample (~300 µl, 36 - 90 mM) was dried on the surface of a Ge internal reflection element and placed in a variable angle ATR accessory (Grasbey Specac, Kent, UK). Fourier self deconvolution spectra [FSD, 22] were obtained using a bandwidth of 13 $cm^{-1}$ and an enhancement factor of 2.4, determined by Byler and Susi [23] to best fit experimental data. The helical content and orientation was determined using the approach described in our recent work on phospholamban [9].

For the SH exchange measurements, samples (400µl) containing 4 mg of dipalmitoyl-phosphatidylcholine (DPPC) and 0.4 mg of protein in a buffer of 0.1 mM $Na_2PO_4$ pH 6.8 were centrifuged for 1 h in an A-95 rotor at 178,000g using an airfuge ultracentrifuge (Beckman, Palo Alto, CA). Pellets were resuspended in 75 µl of either $H_2O$ or $D_2O$ and dried down on germanium IR windows following the procedure of Arkin et al. [31].

*Magic Angle Spinning NMR Spectroscopy.* Magic angle spinning NMR experiments were performed on a Chemagnetics CMX 360 MHz spectrometer using a 5 mm high speed double resonance probe from Doty Scientific (Columbia, SC). The sample spinning speed for the rotational resonance experiments was kept constant to within 5 Hz using a spinning speed controller from Doty Scientific. The temperature was maintained at ca. +5°C or -50°C in order to slow residual rotational diffusion of the peptide which might otherwise average the dipolar couplings being measured. The pulse sequence used for the RR NMR experiments has been described previously [18]. Briefly, the sequence begins with $^1H$-$^{13}C$ cross polarization to generate $^{13}C$ polarization that is then stored on the Z axis with a $^{13}C$ flip-back pulse. One of the two $^{13}C$ resonances is selectively inverted with a low power 500 µsec pulse and magnetization is allowed to exchange between the two sites for a variable

mixing period ($t_m$). The power level of the inversion pulse is carefully adjusted to yield the maximum inversion. The distribution of $^{13}C$ signal at the end of the mix period is detected with a 90° pulse that flips the magnetization into the transverse plane for acquisition of the NMR signal. Strong $^{1}H$ decoupling is essential during the variable mix and acquisition periods. The decoupling power was set to a field strength of 83 kHz during the variable delay and acquisition. This level of decoupling was sufficient to maximize RR exchange as determined by a comparison of exchange rates at different decoupling field strengths. Conventional single amplitude CP was replaced by variable amplitude cross polarization (VACP) for these experiments to enhance the carbon signals at high MAS frequencies and yield more reliable intensities [32]. During the 5 msec CP contact time, the $^{13}C$ amplitude corresponded to a constant spin-lock frequency of ~70 kHz, while the proton amplitude was varied in nine steps each 555 msec in length. The first proton amplitude was centered at a $B_1$ field strength of 70 kHz and the additional amplitudes were increased or decreased in ~2 kHz steps. The VACP sequence yields stable and reproducible signals that are essential for generating the difference spectra and the magnetization exchange curves used for determining internuclear distances.

*Molecular Dynamics Simulations and Energy Minimization.* Molecular dynamics and energy minimization procedures were used to generate structural models of neuTM and neu*TM [32]. Hydrogen atoms were introduced using the CHARMM22 parameter set with electrostatic and van der Waals energy terms enabled using the program X-PLOR in order to insure energetically reasonable initial positions for the hydrogen atoms.

## Assumptions

There are two assumptions that are implicit in the design of the proposed research project.

Assumption 1. Peptides corresponding to the transmembrane sequence (plus ~10 residues on each side) mimic the structure of the transmembrane sequence in the intact receptor. The basis for this assumption is that the hydrophobic environment of the lipid bilayer controls the folding of the transmembrane sequence. As a result, the transmembrane sequence can be considered a protein domain whose structure is independent of the soluble domains of the protein, whose folding is controlled by an aqueous environment.

Assumption 2. The mechanism of dimerization of the transmembrane peptides is the same as that in the intact receptor. Support for this assumption must come from a comparison of the structural results on the transmembrane peptides with the biochemical/molecular biological results on the full length receptor. The structure we propose is consistent with the current literature on the full length receptor *and* provides the basis for the design of additional biochemical experiments.

## Procedures

*Reconstitution of neuTM and neu*TM.* Reconstitution of the peptide fractions into membranes is a critical step in the structural studies undertaken in this research project. Simply put, if the reconstituted peptide does not adopt a well-folded structure, then any structural measurements are worthless. As a result considerable time was placed into refining our reconstitution protocol. Two general reconstitution methods were tried and evaluated using polarized FTIR. The first method simply involved cosolubilization of purified lyophilized peptide and lipid in organic solvent, usually trifluoroethanol (TFE). The lipid-peptide solution was directly layered on the IR plate and the organic

solvent was evaporated. Two variations of this method involved rehydration of the lipid-peptide film, followed by brief sonication before layering on the IR plate, and rehydration, sonication and incubation above the lipid phase transition.

The second reconstitution method involved detergent dialysis. In this case, lipid, peptide (lyophilized) and detergent (octyl-ß-glucoside) were dissolved in trifluoroethanol (TFE). The TFE solution was lyophilized and the dry lipid/peptide/detergent mixture was rehydrated with phosphate buffer (10 mM phosphate and 50 mM NaCl, pH 7), such that the final concentration of octyl-ß-glucoside was 5%. The rehydrated sample was stirred slowly for at least 6 h and then the octyl-ß-glucoside was dialyzed using Spectra-Por dialysis tubing (3000 MW cutoff) for 24 hours against phosphate buffer at a temperature above the lipid phase transition. The reconstituted membranes were sonicated briefly (30-60 sec) in a ultrasonic bath and layered on a germanium crystal for IR measurements. An extension of the second method involved purification of the reconstituted membranes a 10%-40% sucrose gradient. Centrifugation was carried out using a Beckman ultracentrifuge at 35,000 rpm (SW 41 rotor) for 8-12 h at 10°C (POPC) or 20°C (DMPC). Generally, the reconstituted membranes form two discrete bands in the sucrose gradient. The upper band has a more homogeneous appearance and a higher lipid:peptide ratio as assessed by FTIR analysis. The lower band has an aggregated appearance and has a lower lipid:peptide ratio. The sucrose in each band was dialyzed against phosphate buffer for 24 hours.

Based on the results of these two approaches, the final protocol that was used for the structural studies leading to our current model was 1) detergent dialysis, 2) followed by sucrose gradients, 3) followed by incubation for 12h. After this last incubation step, 300 µl of each sample were allocated for ATR-FTIR, approximately 100 µl used for transmission IR, and the remaining pelleted and prepared for MAS-NMR experiments.

*Fourier Transform Infrared Spectroscopy.* The experimental design of the SH exchange experiment has been described previously [31]. Samples (400µl) containing 4 mg of dipalmitoyl-phosphatidylcholine (DPPC) and 0.4 mg of protein in a buffer of 0.1 mM $Na_2PO_4$ pH 6.8 were centrifuged for 1 h in an A-95 rotor at 178,000g using an airfuge ultracentrifuge (Beckman, Palo Alto, CA). Pellets were resuspended in 75 µl of either $H_2O$ or $D_2O$ and dried down on germanium IR windows following the procedure of Arkin et al. [31].

*Magic Angle Spinning NMR Spectroscopy.* The experimental design of the rotational resonance experiment has been described previously [18]. Briefly, the sequence begins with $^1H$-$^{13}C$ cross polarization to generate $^{13}C$ polarization that is then stored on the Z axis with a $^{13}C$ flip-back pulse. One of the two $^{13}C$ resonances is selectively inverted with a low power 500 µsec pulse and magnetization is allowed to exchange between the two sites for a variable mixing period ($t_m$). The power level of the inversion pulse is carefully adjusted to yield the maximum inversion. The distribution of $^{13}C$ signal at the end of the mix period is detected with a 90° pulse that flips the magnetization into the transverse plane for acquisition of the NMR signal. Strong $^1H$ decoupling is essential during the variable mix and acquisition periods. The decoupling power was set to a field strength of 83 kHz during the variable delay and acquisition. This level of decoupling was sufficient to maximize RR exchange as determined by a comparison of exchange rates at different decoupling field strengths. Conventional single amplitude CP was replaced by variable amplitude cross polarization (VACP) for these experiments to enhance the carbon signals at high MAS frequencies and yield more reliable intensities [32]. During the 5 msec CP contact time, the $^{13}C$ amplitude

corresponded to a constant spin-lock frequency of ~70 kHz, while the proton amplitude was varied in nine steps each 555 msec in length. The first proton amplitude was centered at a $B_1$ field strength of 70 kHz and the additional amplitudes were increased or decreased in ~2 kHz steps. The VACP sequence yields stable and reproducible signals that are essential for generating the difference spectra and the magnetization exchange curves used for determining internuclear distances.

*Molecular Dynamics Simulations and Energy Minimization.* The computational search strategy has been described previously by Adams et al. [32]. Low energy conformations of helix dimers were searched by rotating each helix through rotation angles phi1 and phi2 from 0 - 360° with a sampling size of 45°. The starting geometries included both left-handed and right-handed crossing angles. Four different runs were carried out for each starting geometry using simulated annealing of all atomic coordinates. The rotation and crossing angles were allowed to vary. The results of the search can be shown on a grid of phi1 and phi2. The initial grid would show points separated by 45°. The final minimized structures, however, migrate from their initial geometries and often "cluster" in low energy wells. The individual structures in each low energy cluster are averaged.

## Results and Discussion

The technical objectives and results of the proposed research are discussed in this section.

**Structure of the neu and neu* transmembrane and juxtamembrane sequences.**

1. *Magic angle spinning NMR spectroscopy.* Internuclear distance measurements were made in membrane bilayers using rotational resonance (RR) and rotational echo double resonance (REDOR) NMR methods to generate high resolution constraints on neu and neu* transmembrane structures.

2. *Polarized IR spectroscopy.* Contact points in the dimer interface were mapped out using cysteine sulfhydryl exchange. The secondary structure and orientation of the neu and neu* juxtamembrane sequences was also established using attenuated total reflection FTIR spectroscopy. Local secondary structure was characterized by site-directed isotope labeling and helix orientation was characterized by amide I dichroism.

3. *Molecular modeling.* Based on the structural constraints obtained by polarized IR and MAS NMR methods, molecular dynamics and energy minimization protocols were used to model the neu and neu* transmembrane domains.

**Technical Objectives 1-3: Structure of the neu and neu* transmembrane and juxtamembrane domains. Years 1-2**

Task 1: Months 1-12: Polarized IR spectroscopy.

Task 2: Months 12-24: Magic angle spinning NMR spectroscopy.

Task 3: Months 1-48: Molecular modeling.

A second set of tasks for proposed for years 2-4 involving the design of competitive inhibitors was not funded.

## Task 1: Polarized IR Measurements on neuTM and neu*TM.

Position 664 is the only established contact point in the neu* dimer. The major thrust of this section of the proposal was to map out the interacting surfaces in the transmembrane dimer and determine whether or not there are multiple contact points. The approach we used involved cysteine sulfhydryl exchange. The basis for the approach is that single cysteines provide unique markers for exchange. The SH groups in helix interfaces are protected from exchange in a manner analogous to the NH groups buried in the interior of soluble proteins. However, SH groups in the lipid interface undergo rapid SH to SD exchange from water which is known to readily permeate the lipid membrane. The SH vibrational mode is located at 2540 - 2590 $cm^{-1}$ away from other protein vibrations and shifts roughly -700 $cm^{-1}$ upon deuteration. The SH group is more acidic and more mobile than the backbone NH, and consequently exhibits faster exchange rates in membrane environments.

The first set of cysteine sulfhydryl exchange studies targeted the helical turns N-terminal to position 664. Cysteines have been incorporated into residues 656, 657, 658 and 661 in peptides with either valine or glutamate at position 664.

AEQRASP-C-TFIIATV-x-GVLLFLILVVVVGILIKRRRYK  x = E OR V

AEQRASPV-C-FIIATV-x-GVLLFLILVVVVGILIKRRRYK

AEQRASPVT-C-IIATV-x-GVLLFLILVVVVGILIKRRRYK

AEQRASPVTFII-C-TV-x-GVLLFLILVVVVGILIKRRRYK

The sequences for the first four peptides that we targeted are given above. All experiments were carried out under reducing conditions. In each case studied, observation of an SH band at 2560 $cm^{-1}$ showed that the samples were reduced.

Figure 2 presents transmission FTIR spectra of the SD region of neu*TM in DPPC membrane bilayers from two sites, position 657 and position 661. The results from the SH exchange studies are easy to interpret. If an SD band appears in $D_2O$, then the site is not buried in a helix interface but exposed to lipid. The absence of an SD band in the A661C neu*TM peptide indicates that position 661 is buried in the dimer interface. This results establishes a second contact point along the dimer interface in the activated neu* receptor. The presence of an SD band in T657C (Figure 2, top) is consistent with this position being oriented towards the surrounding lipids. SD bands were also observed with the V656C and F658C neu*TM peptides (data not shown).

Measurements on both neu and neu* sequences with cysteine substitutions on the C-terminal side of position 664 were also undertaken. Four sites were targeted as shown on the sequences below. Each cysteine replaced a native valine in the sequence resulting in substitutions around one helical turn. As a result, a cysteine residue should reside on each face in the C-terminal portion of the neu transmembrane domain.

AEQRASPVTFIIATV-x-GVLLFLIL-C-VVVGILIKRRRYK x = E OR V

AEQRASPVTFIIATV-x-GVLLFLILV-C-VVGILIKRRRYK

AEQRASPVTFIIATV-x-GVLLFLILVV-C-VGILIKRRRYK

AEQRASPVTFIIATV-x-GVLLFLILVVV-C-GILIKRRRYK

In contrast to the results above, all four sites exhibited significant exchange suggesting that none of the four sites are packed in a helix interface. These results are incorporated and discussed in the computational search and modeling section below (Task 3).

## Task 2: Magic Angle Spinning NMR Measurements of Intra- and Interhelical Contacts in neu*TM.

The aim of the studies described in this section was to obtain distance constraints for the molecular modeling studies described under Task 3. We first describe measurements between $^{13}C$ labels incorporated into the neu and neu* transmembrane sequences in the vicinity of position 664. The spacing of the labels is sensitive to the transmembrane secondary structure.

Figure 3 presents the results of the intra-peptide RR NMR experiments. The experimental design of these experiments was described above in the *Procedures* section. The key data comes from the changes in intensity of the two $^{13}C$ resonances. Large intensity changes correspond to short distances and small intensity changes correspond to long distances. The results are displayed as magnetization exchange curves which plot the normalized intensity differences between the two $^{13}C$ resonances as a function of a mixing time. Figure 3a presents the magnetization exchange curves of [1-$^{13}$C-Gly$^{665}$, 3-$^{13}$C-Ala$^{668}$] neuTM and neu*TM. In a canonical helix, these $^{13}C$-labels are separated by ~4.5 Å. Simulations of the magnetization exchange are shown with solid lines for internuclear distances of 4.0, 4.5 and 5.0 Å using a zero quantum $T_2$ of 1.6 ms.

Figure 3b presents the magnetization exchange curves of [1-$^{13}$C-Thr$^{662}$, 2-$^{13}$C-Gly$^{665}$] neuTM and neu*TM. In a canonical helix, these $^{13}C$-labels are separated by ~4.8 Å. Simulations of the magnetization exchange are shown with solid lines for internuclear distances of 4.0, 4.5 and 5.0 Å using a zero quantum $T_2$ of 1.2 ms. The shorter zero quantum $T_2$ value reflects the fact that the methylene $CH_2$ group is harder to decouple than a methyl group. The zero quantum $T_2$ parameter in general reflects intensity changes in the lines that are *not* due to the rotational resonance phenomenon. The values we have used were taken from independent spin echo linewidths. The fact that the simulations predict distances that are slightly shorter than those we expected for canonical helices is likely due to the fact that the zero quantum $T_2$ parameter is underestimated. This places an error of ±0.3 Å on all of the measurements in this study.

One of the goals of the proposed research was to test various models for the structure of neu*TM and the structural changes occurring between neuTM and neu*TM. The first model mentioned in the introduction involved a change in the secondary structure of the transmembrane domain between neuTM and neu*TM. Brandt-Rauf et al. [5] calculated that the minimum-energy conformation of neuTM contains a sharp bend at positions 664 and 665, neu*TM exists as an α-helix.

The intrahelical rotational resonance measurements discussed here have ruled out such a change in secondary structure.

Two additional models for receptor activation involve dimerization via hydrogen-bonding interactions [6]. In the first model, the helices are thought to be held in the "active" state by hydrogen bonding between the $Glu^{664}$ COOH side chain on one helix and the $Glu^{664}$ COOH side chain on the opposing helix. In the second model, the hydrogen bonding interactions are postulated to be between the $Glu^{664}$ side chain and the peptide backbone carbonyl group of $Ala^{661}$ of the second helix. The first set of interhelical measurements were aimed at the interaction between the $Glu^{664}$ side chain and $Gly^{665}$.

Figure 4 presents the interhelical RR magnetization exchange curves for [5-$^{13}$C-$Glu^{664}$] neu*TM reconstituted with [2-$^{13}$C-$Gly^{665}$] neu*TM. The peptides were reconstituted in a 1:5 ratio and only the COOH intensity is plotted in Figure 4. This insures that ~85% of each [5-$^{13}$C-$Glu^{664}$] neu* peptide interacts with a [2-$^{13}$C-$Gly^{665}$] neu*TM peptide. Using the reconstitution protocol that involved detergent dialysis and sucrose gradients (but without incubation above the phase transition temperature), the data (solid circles) appear to be biphasic with a fast (~4 Å distance) and a slow component (> 5.5 Å distance). There are two possible explanations for this observation. First, the two glutamic acid groups in the dimer may have different conformations and correspondingly different distances to $Gly^{665}$. The second possibility is that there are two (or more) dimer structures, one where the Glu - Gly distance is short and one where the distance is long. The idea in the second case is that one of the conformations is thermodynamically or kinetically trapped. To address this case, we incubated the sample above the phase transition temperature. Measurements after (open circles) incubation above the phase transition temperature of DMPC shows only the slow component. Simulations of the magnetization exchange are shown with solid lines for internuclear distances of 3.5, 4.0, 4.5 and 5.0 Å using a zero quantum $T_2$ of 1.2 ms.

Based on the dimer structure of glycophorin A where glycine residues are critical for dimerization (33), we targeted the distance between Gly residues across the dimer interface. Glycine has no side chain and potentially provides good van der Waals packing. Figure 5 presents interhelical RR magnetization exchange curves for [2-$^{13}$C-$Gly^{665}$] neu*TM reconstituted with [1-$^{13}$C-$Gly^{664}$] neu*TM (solid circles) and with wild-type [1-$^{13}$C-$Gly^{664}$] neuTM (open circles) in a 1:5 molar ratio. The neuTM - neu*TM experiments were designed to test whether the mutant TM domain was also able to interact with the wild-type TM domain. Experiments were run after incubation for 12 h above the DMPC phase transition temperature. The Gly - Gly distance of 4 - 4.5 Å appears only slightly longer in the neu-neu* heterodimer than in the neu* homodimer. RR intensity changes of [2-$^{13}$C-$Gly^{665}$] neu*TM reconstituted with [1-$^{13}$C-$Gly^{664}$] neu*TM before incubation are shown in open squares. Simulations of the magnetization exchange are shown with solid lines for internuclear distances of 3.5, 4.0, 4.5 and 5.0 Å using a zero quantum $T_2$ of 1.2 ms.

To further constrain the packing arrangement of the glycine residues in the interface, we also made RR measurements of [2-$^{13}$C-$Gly^{665}$] neu*TM reconstituted with [1-$^{13}$C-$Ala^{661}$] neu*TM in a 1:5 molar ratio. The data are plotted in Figure 6 and correspond to an internuclear distance of ~5 Å. The calculated distances in the structure proposed below are 4.1 and 7.4 Å.

Finally, the Gly-Gly experiments described above provide an indication as to the packing interface in neu*, but do not address nature of the hydrogen-bonding partner or partners of $Glu^{664}$.

One possibility that emerged from the modeling studies below is that $Glu^{664}$ may be hydrogen-bonded to the polar threonine side chains at positions 657 and/or 662. Figure 7 presents RR magnetization exchange curves of [U-$^{13}$C-$Thr^{662}$, 5-$^{13}$C-$Glu^{664}$] neu*TM reconstituted in DMPC. Simulations of the magnetization exchange are shown with solid lines for internuclear distances of 4.0, 4.5 and 5.0 Å using a zero quantum $T_2$ of 1.6 ms. The measurements were made after incubation for 12 h and the estimated internuclear distance of 4.5 - 5 Å is shorter than the 5 - 6 Å internuclear distance between $Glu^{664}$ and $Gly^{665}$ shown in Figure 4 after incubation.

The distances between the $^{13}$C-labels discussed above are summarized in Table I in the appendix section.

## Task 3. Computational Searches for the neu*TM Dimer Interface.

A. Brünger and coworkers have developed a computational search strategy for locating low energy conformations of dimers of transmembrane helices [32]. The approach has been used to locate the dimer interface between transmembrane helices of glycophorin A [33]. Low energy conformations of helix dimers are searched by rotating each helix through rotation angles phi1 and phi2 from 0 - 360° with a sampling size of 45°. The starting geometries include both left-handed and right-handed crossing angles.

Figure 8 presents the results of a computational search for the neu*TM interface. This figure shows the cluster plot of low energy structures having left-handed crossing angles. Five left-handed clusters have been identified based on their final phi1 and phi2 angles, as well as their interaction energies and crossing angles. The initial grid, if shown, would display points separated by 45°. Figure 8 shows only those points that fall into a "cluster". These are the final minimized conformations that have migrated from their initial geometries and into low energy wells.

Figure 9 shows the low energy structures having right-handed crossing angles. Two right-handed clusters have been identified.

The orientations of $Glu^{664}$ (red) and $Gly^{665}$ (yellow) for each of the seven clusters (both left and right-handed structures) are shown in Figure 10 (viewed down the helix axis of the one of the monomers in the dimer). Both $Glu^{664}$ and $Gly^{665}$ might be expected to be in the interface based on the mutagenesis studies of Stern and coworkers [4]. Two clusters (cluster 4 and 7) are roughly symmetric. The interaction energy of cluster 7 at -126.2 kcal/mole is much lower than that of cluster 4. In these simulations the dielectric constant is assumed to be $\varepsilon$=2 and the interaction energy is driven by helix-helix interactions (both favorable and unfavorable).

Three parameters make up the input for any given computational search: the peptide sequence, the sampling step size and the helix-helix separation. The initial searches start with a step size of 45°, but this is narrowed once candidate clusters have been identified. The helix-helix separation can range from ~10.0 - 11.5 Å. The calculations shown in Figures 8-10 are based on a helix-helix separation of 10.5 Å. Helix-helix separations of 11.0 and 11.5 Å gave similar results, however with a separation of 10.0 Å the $Glu^{664}$ side chains did not interact with the opposing helix.

Figure 11 presents the low energy structures of neuTM and neu*TM homodimers. (For neu*TM, this is cluster 7 in Figures 9 and 10). In both cases the low energy structure predicts that

$Gly^{665}$ packs in the dimer interface. In neuTM (with valine at position 664), this is a left-handed coiled coil, while for neu*TM a right-handed geometry is predicted. The most stabilizing interactions in neu*TM come from interhelical hydrogen-bonding of the $Glu^{664}$ carboxyl side side with the hydroxyl side chains of $Thr^{657}$ and $Thr^{662}$. The structure is not completely symmetric. Hydrogen-bonding of $Glu^{664}$ with Thr662 is supported by the rotational resonance NMR measurements in Figure 7. The neu*TM structure in Figure 11 is also consistent with the SH exchange data which show that position 661 is buried in the dimer interface and unable to exchange. The position of Ala661 (purple) in the dimer interface is shown in Figure 12b. A small residue at this position appears to be a conserved feature of growth factor receptors in the receptor tyrosine kinase family.

Figure 13 again presents the low energy structure of neu*TM homodimer. The inset shows the neu*TM dimer with a 40° crossing angle in agreement with our polarized IR measurements. The relatively large crossing angle is thought to facilitate orientation of the intracellular kinase domains. The comparison of the distances obtained by experiment and by computational searching show that we are not far off. This parallel approach bolsters our confidence in the results of both the NMR measurements and the computational searches.

## CONCLUSIONS

The objective of the DAMD grant was to establish high resolution structural constraints on the transmembrane domain of the neu/erbB-2 receptor in membrane environments. Such data addresses specific models for receptor activation by the transforming $Glu^{664}$ mutation and provides a basis for the design of competitive inhibitors. The conclusions that can be drawn are as follows:

- $Glu^{664}$ drives the dimerization of the neu* transmembrane domain through hydrogen-bonding inteactions.
- $Glu^{664}$ interacts with or is at the level of the phospholipid headgroups. We can observe weak dipolar couplings between the $^{31}P$ site of the lipid phosphate and the 5-$^{13}COOH$ of $Glu^{664}$.
- $Gly^{665}$ and $Ala^{661}$ pack in the dimer interface and stabilize the helix dimer through van der Waals interactions.
- The polar threonine residues at positions 662 and 657 may be involved in stabilizing the active neu* dimer through hydrogen bonding interactions.
- The observation of deuterium exchange of the four cysteine sites in the C-terminus of the neu transmembrane domain is consistent with a large helix crossing angle.
- Computational searches predict a left-handed geometry for the neu transmembrane sequence and a right-handed geometry for neu* transmembrane sequence.
- The secondary structure of the neu and neu* transmembrane sequences is the same. The activating mutation does not induce a large change in secondary structure.

In terms of designing competitive inhibitors, two major conclusions can be drawn from these studies thus far.

- Specific inhibitors to the neu* sequence should target the polar threonine and glutamic acid residues as well as the van der Waals surfaces created by $Gly^{665}$ and $Ala^{661}$, both of which have small side chains and allow good packing interactions.
- Specific inhibitors to the neu sequence should target the polar threonine residues as well as $Gly^{665}$ and $Ala^{661}$. Inhibitors to the neu sequence are of importance because overexpression of the wild-type receptor leads to receptor activation. The observation that $Gly^{665}$ is likely in the dimer interface of both neu and neu* is consistent with a common orientation and mechanism of activation.

## REFERENCES


1 Bargmann CI, Weinberg RA. Oncogenic activation of the neu-encoded receptor protein by point mutation and deletion. EMBO J 1988; 7:2043-2052.

2 Bargmann CI, Hung M-C, Weinberg RA. Multiple independent activations of the neu oncogene by a point mutation altering the transmembrane domain of p185. Cell 1986; 45:649-657.

3 Bargmann CI, Hung M-C, Weinberg RA. The neu oncogene encodes an epidermal growth factor receptor-related protein. Nature 1986; 319:226-230.

4 Cao H, Bangalore L, Bormann B-J, Stern DF. A subdomain in the transmembrane domain is necessary for p185neu* activation. EMBO J 1992; 11:923-932.

5 Brandt-Rauf PW, Rackovsky S, Pincus MR. Correlation of the structure of the transmembrane domain of the neu oncogene-encoded p185 protein with its function. Proc Natl Acad Sci U S A 1990; 87:8660-8664.

6 Sternberg MJ, Gullick WJ. Neu receptor dimerization. Nature 1989; 339:587.

7 Weiner DB, Liu J, Cohen FA, Williams WV, Greene MI. Nature 1989; 339:230-231.

8 Lofts FJ, Hurst HC, Sternberg MJE, Gullick WJ. Specific short transmembrane sequences can inhibit transformation by the mutant neu growth factor receptor in vitro and in vivo. Oncogene 1993; 8:2813-2820.

9 Arkin IT, Rothman M, Ludlam CFC, Aimoto S, Engelman DE, Rothschild K, Smith SO. Structural model of the phospholamban ion channel complex in phospholipid membranes. J Mol Biol 1995; 248:824-834.

10 Smith SO, Jonas R, Braiman M, Bormann BJ. Structure and orientation of the transmembrane domain of glycophorin A in lipid bilayers. Biochemistry 1994; 33:6334-6341.

11 Smith SO, Bormann BJ. Determination of helix-helix interactions in membranes by rotational resonance NMR. Proc Natl Acad Sci USA 1995; 92:488-491.

12. Levitt MH, Raleigh DP, Creuzet F, Griffin RG. Theory and simulations of homonuclear spin pair systems in rotating solids. J Chem Phys 1990; 92:6347.

13 Gullion T, Schaefer J. Detection of weak heteronuclear dipolar coupling by rotational echo double-resonance nuclear magnetic resonance. Adv Magn Reson 1989; 13:57-83.

14 Hing AW, Vega S, Schaefer J. Transferred-echo double resonance NMR. J Magn Reson 1992; 96:205-209.

15 Tycko R, Smith SO. Symmetry principles in the design of pulse sequences for structural measurements in magic angle spinning nuclear magnetic resonance. J Chem Phys 1993; 98:932-943.

16 Colombo MG, Meier BH, Ernst RR. Rotor-driven spin diffusion in natural-abundance 13-C Spin Systems. Chem Phys Lett 1988; 146:189-196.

17 Peersen OB, Yoshimura S, Hojo H, Aimoto S, Smith SO. Short range distance determination in integral membrane proteins by magic angle spinning NMR. J Am Chem Soc 1992; 114:4332-4335.

18 Peersen OB, Groesbeek, M, Aimoto, S., Smith SO. Analysis of rotational resonance magnetization exchange curves from crystalline peptides 1995; 117:7228-7237.

19 Bork V, Gullion T, Hing A, Schaefer J. Measurement of 13-C - 15-N coupling by dipolar-rotational spin-echo NMR. J Magn Reson 1990; 88:523-532.

20 Gullion T, Schaefer J. Rotational-Echo Double-Resonance NMR. J Magn Reson 1988; 81:196-200.

21 Braiman MS, Rothschild KJ. Fourier transfrom infrared techniques for probing membrane protein structure. Ann Rev Biophys Biophys Chem 1989; 17:541-570.

22 Kauppinen JK, Moffatt DJ, Mantsch HH, Cameron DG. Fourier self-deconvolution: A method for resolving intrinsically overlapped bands. Appl Spectrosc 1981; 35:271-276.

23 Byler MD, Susi H. Examination of the secondary structure of proteins by Deconvolved FTIR spectra. Biopolymers 1986; 25:469-487.

24 Bradbury EM, Brown L, Downie AR, Elliott A, Fraser RDB, Hanby WE. The structure of the ω-form of poly-β-benzyl-L-aspartate. J Mol Biol 1962; 5:230247.

25 Miyazawa T, Blout ER. The infrared spectra of polypeptides in various conformations: amide I and amide II bands. J Am Chem Soc 1961; 83:712-719.

26 Tsuboi M. Infrared dichroism and molecular conformation of α-form poly-γ-benzyl-L-glutamate. J Polymer Sci 1994; 59:139-153.

27 Gu Z, Zambrano R, McDermott A. Hydrogen bonding of carboxyl groups in solid-state amino acids and peptides: comparison of carbon chemical shielding, infrared frequencies, and structures. J Am Chem Soc 1994; 116:6368-6372.

28 Hamilton JA, Cistola DP. Transfer of oleic acid between albumin and phospholipid vesicles. Proc Natl Acad Sci USA 1986; 83:82-86.

29 Kantor HL, Prestegard JP. Fusion of phosphatidylcholine bilayer vesicles: role of free fatty acid. Biochemistry 1978; 17:3592-3597.

30 Ptak M, Egret-Charlier M, Sanson A, Bouloussa O. A NMR study of the ionization of fatty acids, fatty amines and N-acylamino acids incorporated in phosphatidylcholine vesicles. Biochim Biophys Acta 600:387-397 (1980).

31 Arkin, I.T., Mackenzie, K., Aimoto, S., Engelman, D. and S.O. Smith Mapping the lipid exposed surface of membrane proteins. Nature Struct. Biol. 3, 240-243 (1996).

32 Adams, PD, Arkin, IT, Engelman, DM, Brunger, AT. Computational searching and mutagenesis suggest a structure for the pentameric transmembrane domain of phospholamban. Nature Struct. Biol. 2, 154-162 (1995).

33. Treutlein, HR, Lemmon, M, Engelman, DM, Brunger, AT. The glycophorin A transmembrane domain dimer: sequence specific propensity for a right-handed supercoil of helices. Biochemistry 31, 12726-12733 (1992).

## Appendix

Table 1

| Sample | Experimental Distance | Calculated Distance |
|---|---|---|
| [1-$^{13}$C-Gly$^{665}$, 3-$^{13}$C-Ala$^{668}$] neu*TM | 4.3-4.4 Å | 4.5 Å |
| [1-$^{13}$C-Gly$^{665}$, 3-$^{13}$C-Ala$^{668}$] neuTM | 4.3-4.4 Å | 4.5 Å |
| [1-$^{13}$C-Thr$^{662}$, 2-$^{13}$C-Gly$^{665}$] neu*TM | 4.5-4.7 Å | 4.8 Å |
| [1-$^{13}$C-Thr$^{662}$, 2-$^{13}$C-Gly$^{665}$] neuTM | 4.5-4.7 Å | 4.8 Å |
| [5-$^{13}$C-Glu$^{664}$] neu*TM <-> [2-$^{13}$C-Gly$^{665}$] neu*TM | > 5.0 Å | 5.8 and 6.5 Å |
| [2-$^{13}$C-Gly$^{665}$] neu*TM <-> [1-$^{13}$C-Gly$^{664}$] neu*TM | 4.0 Å | 4.1 Å |
| 2-$^{13}$C-Gly$^{665}$] neu*TM <-> [1-$^{13}$C-Gly$^{664}$] neuTM | 4.4 Å | 4.2 Å |
| [2-$^{13}$C-Gly$^{665}$] neu*TM <-> [1-$^{13}$C-Ala$^{661}$] neu*TM | 4.5 - 5.0 Å | 4.1 and 7.4 Å |
| [$CH_3$-$^{13}$C-Thr$^{662}$, 5-$^{13}$C-Glu$^{664}$] neu*TM | 4.2 - 5.0 Å | 4.4 and 6.3 Å |

## Figure Legends

Figure 1: Helical wheel diagram of the erbB-2 transmembrane domain. Residues from $Leu^{670}$ to $Ala^{653}$ are shown in a canonical α-helix having 3.6 residues per turn.

Figure 2: Polarized transmission FTIR spectra of the SD region of neu*TM in DPPC membrane bilayers. Cysteine substitutions were made at Thr 657 (a) and at Ala 661 (b). The absense of an SD band in the A661C neu*TM peptide suggests that position 661 is buried in the dimeri interface. The sample chamber was purged with nitrogen, and the samples layered on a Ge crystal plate and dried using argon or nitrogen. Each spectrum represents the average of 1000 scans acquired at a resolution of 4 $cm^{-1}$.

Figure 3: Intrahelical $^{13}C$ RR magnetization exchange curves. (a) Intensity differences of [1-$^{13}$C-$Gly^{665}$, 3-$^{13}$C-$Ala^{668}$] neuTM and neu*TM peptides as a function of mixing time. In a canonical helix, these $^{13}C$-labels are separated by ~4.5 Å. Simulations of the magnetization exchange are shown with solid lines for internuclear distances of 4.0, 4.5 and 5.0 Å using a zero quantum $T_2$ of 1.6 ms. (b) Intensity differences of [1-$^{13}$C-$Thr^{662}$, 2-$^{13}$C-$Gly^{665}$] neuTM and neu*TM peptides as a function of mixing time. In a canonical helix, these $^{13}C$-labels are separated by ~4.8 Å. Simulations of the magnetization exchange are shown with solid lines for internuclear distances of 3.5, 4.0, 4.5 and 5.0 Å using a zero quantum $T_2$ of 1.2 ms.

Figure 4: Interhelical RR magnetization exchange curves for neu*TM. RR intensity changes of [5-$^{13}$C-$Glu^{664}$] neu*TM reconstituted with [2-$^{13}$C-$Gly^{665}$] neu*TM. Measurements were made before (solid circles) and after (open circles) incubation above the above the phase transition temperature of DMPC. Before incubation the curves appear to be biphasic with a fast (~4 Å distance) and a slow component (> 5.5 Å distance). The fast component disappears upon incubation. Simulations of the magnetization exchange are shown with solid lines for internuclear distances of 3.5, 4.0, 4.5 and 5.0 Å using a $T_2zq$ of 1.2 ms.

Figure 5: Interhelical RR magnetization exchange curves for neu*TM-neu*TM and neu*TM-neuTM dimers. RR intensity changes of [2-$^{13}$C-$Gly^{665}$] neu*TM reconstituted with [1-$^{13}$C-$Gly^{665}$] neu*TM (solid circles) and with wild-type [1-$^{13}$C-$Gly^{665}$] neuTM (open circles) in a 1:5 molar ratio. Experiments were run after incubation for 12 h above the DMPC phase transition temperature. The Gly - Gly distance of 4 - 4.5 Å appears only slightly longer in the neu-neu* heterodimer than in the neu* homodimer. RR intensity changes of [2-$^{13}$C-$Gly^{665}$] neu*TM reconstituted with [1-$^{13}$C-$Gly^{665}$] neu*TM before incubation are shown in open squares. Simulations of the magnetization exchange are shown with solid lines for internuclear distances of 3.5, 4.0, 4.5 and 5.0 Å using a zero quantum $T_2$ of 1.2 ms.

Figure 6: Interhelical rotational resonance NMR magnetization exchange curves for neu*TM. (a) RR intensity changes of [2-$^{13}$C-$Gly^{665}$] neu*TM reconstituted with [1-$^{13}$C-$Gly^{665}$] neu*TM in a 1:5 molar ratio. The internuclear distance is estimated to be ~4 Å close to the 4.06 Å distance in the calculated structure. (b) RR intensity changes of [2-$^{13}$C-$Gly^{665}$] neu*TM reconstituted with [1-$^{13}$C-$Ala^{661}$] neu*TM in a 1:5 molar ratio. The internuclear distance is estimated to be ~5 Å. The calculated distances in the structure proposed below are 4.1 and 7.4 Å. Simulations are shown in both curves for internuclear distances of 3.5, 4.0, 4.5 and 5.0 Å using a zero quantum $T_2$ of 1.2 ms.

Figure 7: RR intensity changes of [U-$^{13}$C-Thr$^{662}$, 5-$^{13}$C-Glu$^{664}$] neu*TM reconstituted in DMPC. Simulations of the magnetization exchange are shown with solid lines for internuclear distances of 4.0, 4.5 and 5.0 Å using a zero quantum $T_2$ of 1.6 ms. The measurements were made after incubation for 12 h and the estimated internuclear distance of 4.5 - 5 Å is shorter than the 5 - 6 Å internuclear distance between Glu$^{664}$ and Gly$^{665}$ shown in Figure 4 after incubation.

Figure 8: Computational search for neu*TM interface. Cluster plot showing low energy structures having left-handed crossing angles.

Figure 9: Computational search for neu*TM interface. Cluster plot showing low energy structures having right-handed crossing angles.

Figure 10: Structures from computational search of neu*TM dimers. Seven clusters were identified. Two clusters (cluster 4 and 7) are roughly symmetric. Interaction energies are listed.

Figure 11: Low energy structures of neuTM and neu*TM homodimers. In both cases the low energy structure predicts that the Gly$^{665}$ packs in the dimer interface.

Figure 13: Low energy structures of the neuTM (a) and neu*TM (b,c) homodimers. Gly 665 (red) and Val 664 (green) pack in the dimer interface in neuTM. In neu*TM both Gly 665 (red) and Ala 661 (purple) pack in the interface. Hydrogen bonding of Glu 664 (green in b and c) across the interface stabilizes the transmembrane dimer.

Figure 13: Low energy structure of the neu*TM homodimer. The inset shows the neu*TM dimer with a 40° crossing angle in agreement with polarized IR measurements.

## BIBLIOGRAPHY AND PERSONNEL

### Publications

1. Smith, S.O., Smith, C.S. and Bormann, B.J. Strong hydrogen bonding interactions involving a buried glutamic acid in the transmembrane domain of the neu/erbB-2 receptor. Nature Struct. Biol. 3, 252-258 (1996).

2. Smith, S.O., Ziliox, M., Surti, T. and Aimoto, S. Transmembrane interactions in the activation of the neu receptor tyrosine kinase. Science, submitted.

3. Smith, S.O., Shekar, S., Peersen, O., Surti, T., Ziliox, M. and Aimoto, S. Structure of the neu (erbB2) receptor transmembrane domain. A moleular hinge in receptor activation. J. Mol. Biol., submitted.

4. Smith, S.O., Shekar, S., Joers, J. and Aimoto, S. Association of transmembrane helices from the neu and neu* receptors. In preparation.

### Abstracts

1. Smith, S.O., Ziliox, M., Surti, T. and Aimoto, S. Transmembrane interactions in the activation of the neu receptor tyrosine kinase. Experimental Nuclear Magnetic Resonance Conference. 1997 Orlando, FL.

2. Smith, S.O., Shekar, S., Peersen, O., Surti, T., Ziliox, M. and Aimoto, S. Structure of the neu (erbB2) receptor transmembrane domain. A moleular hinge in receptor activation. Experimental Nuclear Magnetic Resonance Conference. 1998 Asilomar, CA

3. Smith, S.O., Ziliox, M., Surti, T. and Aimoto, S. Transmembrane interactions in the activation of the neu receptor tyrosine kinase. DAMD Breast Cancer Meeting. November 1997. Washington, D.C.

### Personnel

| | |
|---|---|
| Steven O. Smith | Principal Investigator |
| Michel Groesbeek | Postdoctoral Associate |
| Melanie Cocco | Postdoctoral Associate |
| James Joers | Postdoctoral Associate |
| Srinivasan Shekar | Postdoctoral Associate |
| Ted Shieh | Technician |
| Toral Surti | Undergraduate |
| Xenia Protopopescu | Undergraduate |

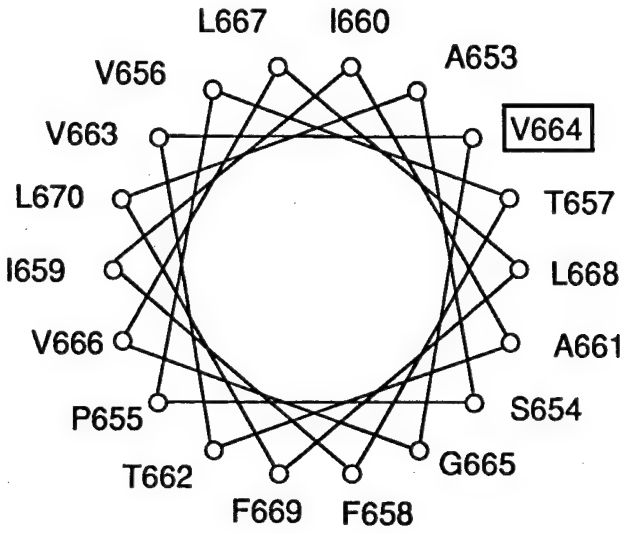


neu (V664)

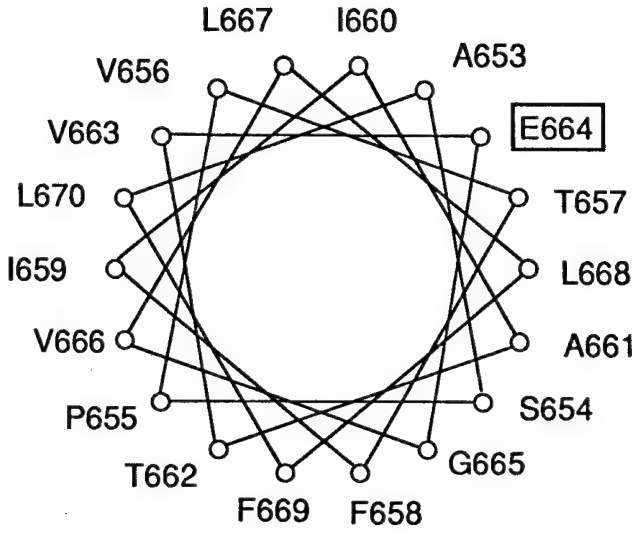


neu* (E664)

FIGURE 1

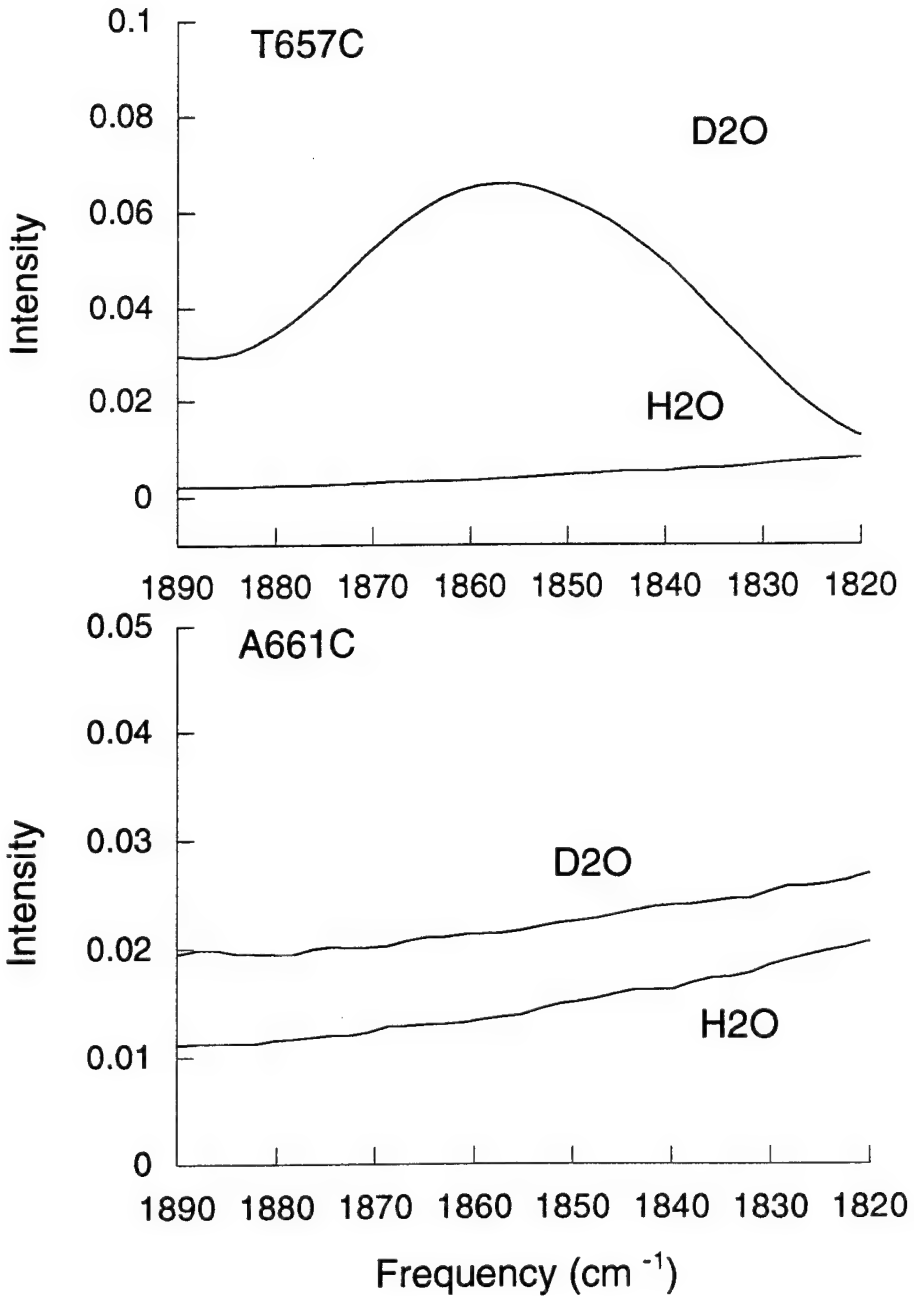
T657C
D2O
H2O
Intensity
0.1
0.08
0.06
0.04
0.02
0
1890 1880 1870 1860 1850 1840 1830 1820
A661C
D2O
H2O
Intensity
0.05
0.04
0.03
0.02
0.01
0
1890 1880 1870 1860 1850 1840 1830 1820
Frequency (cm -1)

FIGURE 2

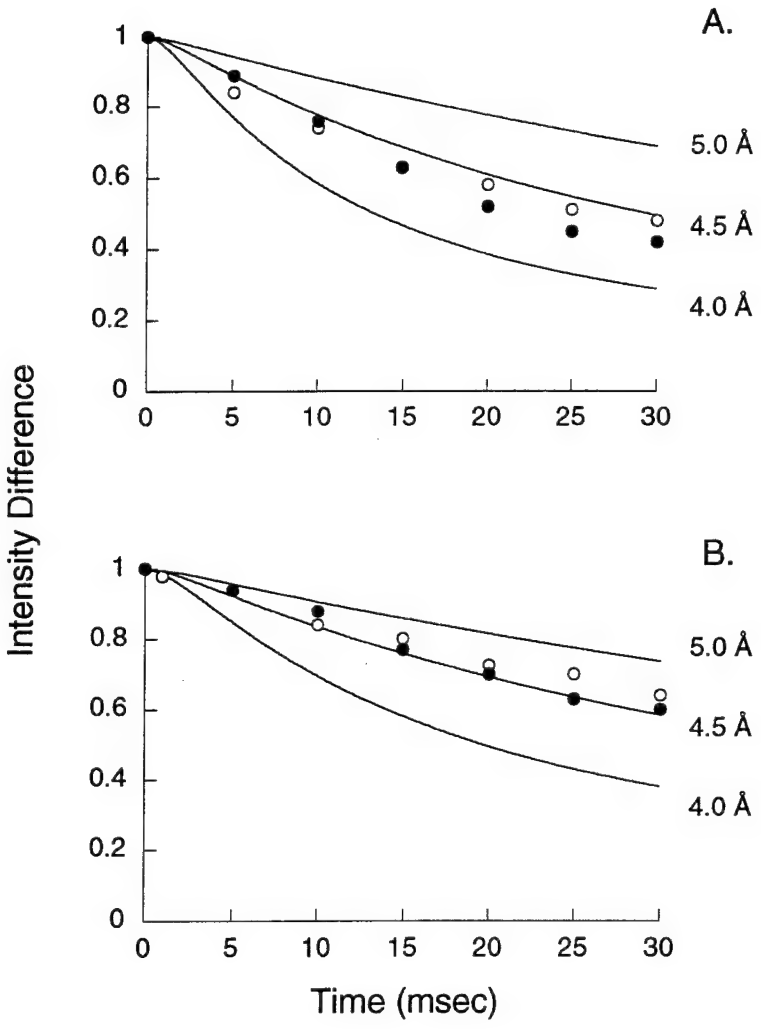
A.
B.
5.0 Å
4.5 Å
4.0 Å
Intensity Difference
Time (msec)
1
0.8
0.6
0.4
0.2
0
0
5
10
15
20
25
30

FIGURE 3

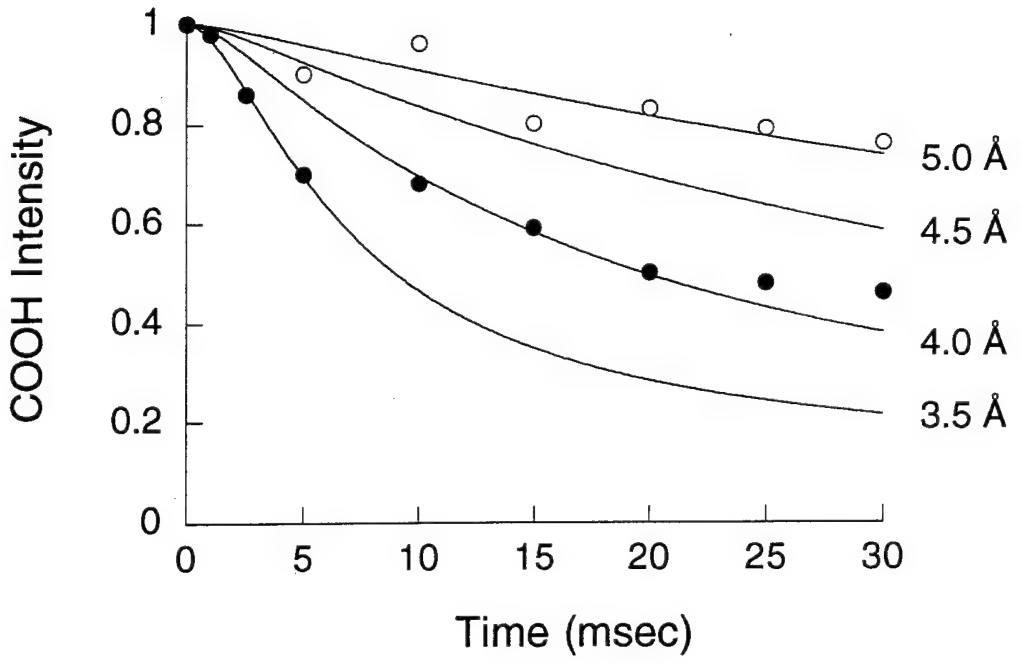
COOH Intensity
1
0.8
0.6
0.4
0.2
0
0
5
10
15
20
25
30
Time (msec)
5.0 Å
4.5 Å
4.0 Å
3.5 Å

FIGURE 4

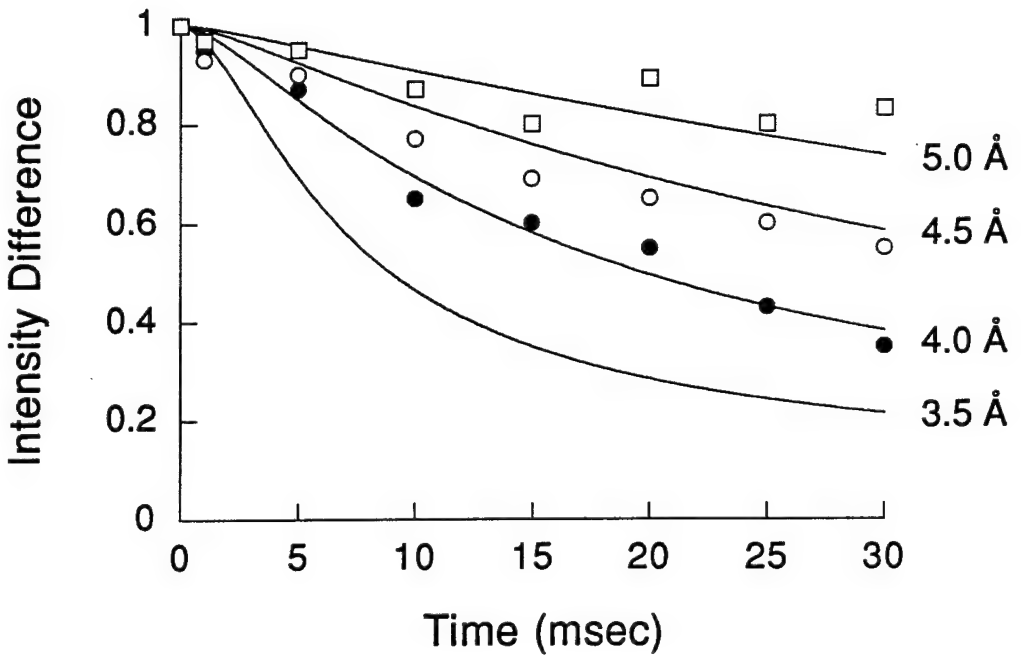
Intensity Difference
1
0.8
0.6
0.4
0.2
0
0
5
10
15
20
25
30
Time (msec)
5.0 Å
4.5 Å
4.0 Å
3.5 Å

FIGURE 5

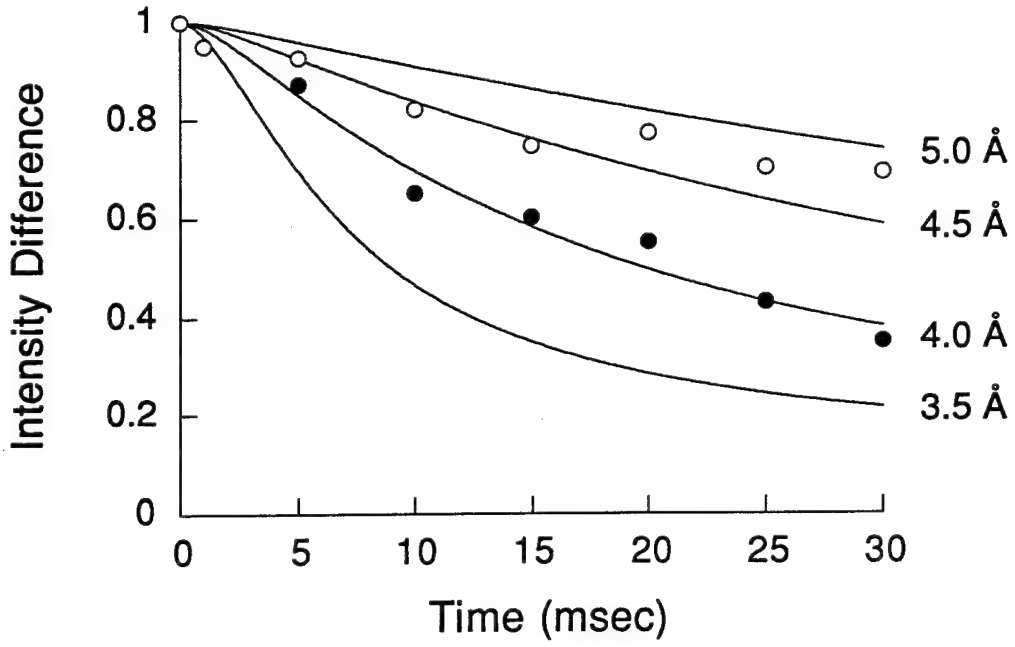
Intensity Difference
1
0.8
0.6
0.4
0.2
0
0
5
10
15
20
25
30
Time (msec)
5.0 Å
4.5 Å
4.0 Å
3.5 Å

FIGURE 6

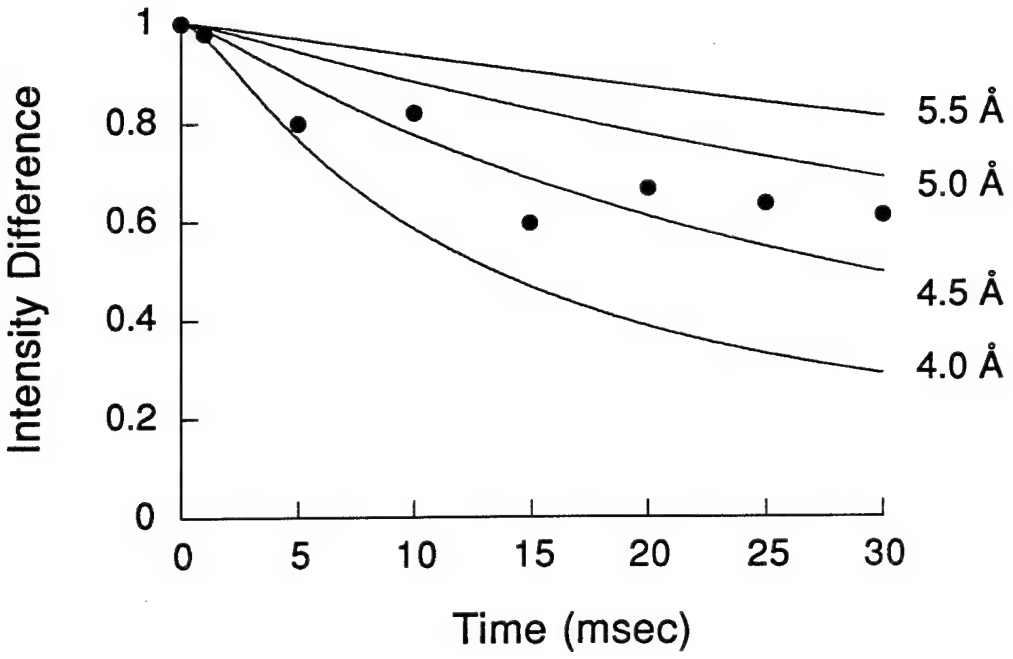
Intensity Difference
1
0.8
0.6
0.4
0.2
0
0
5
10
15
20
25
30
Time (msec)
5.5 Å
5.0 Å
4.5 Å
4.0 Å

FIGURE 7

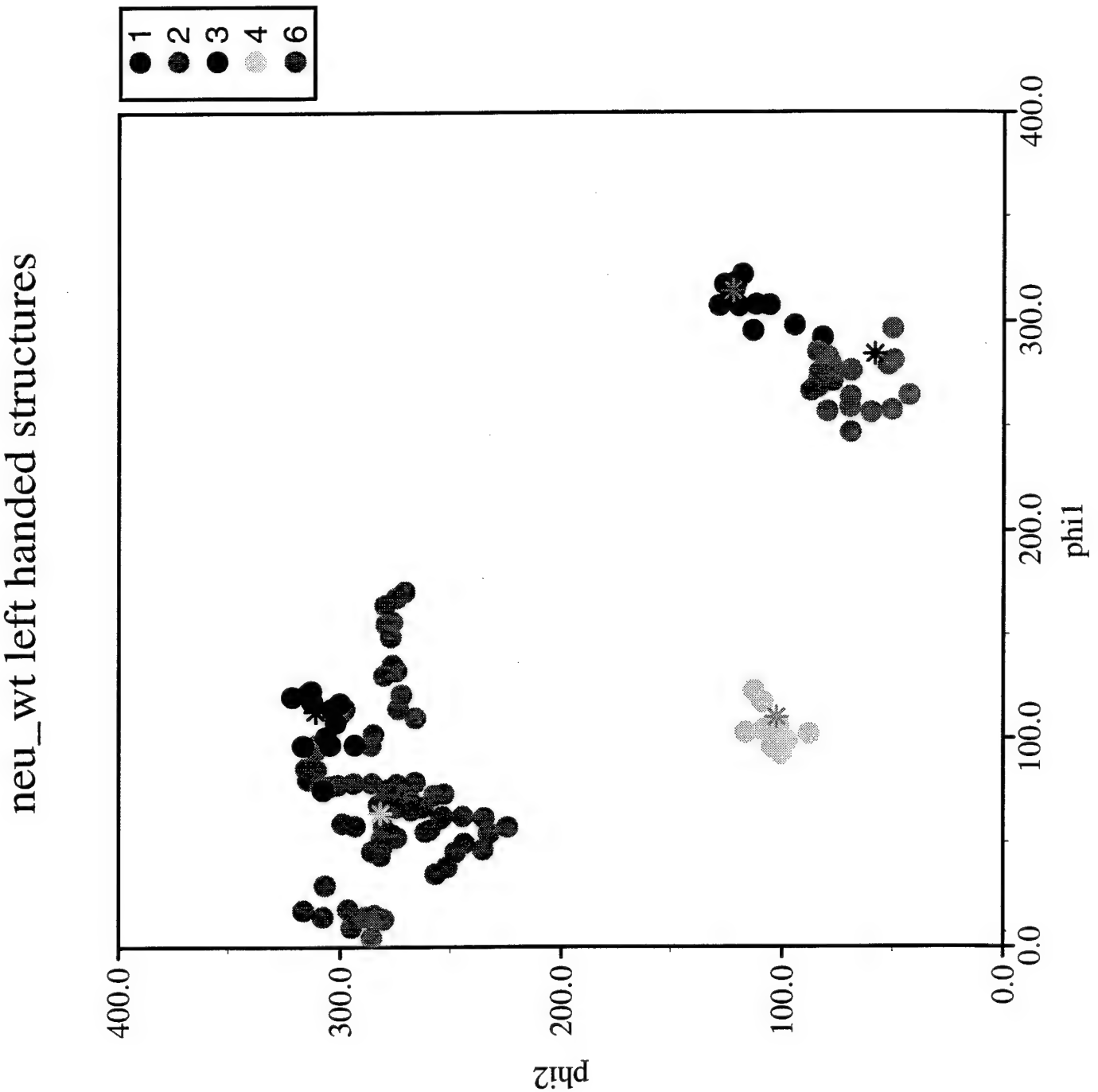
neu_wt left handed structures
1
2
3
4
6
400.0
300.0
200.0
100.0
0.0
phi2
0.0
100.0
200.0
300.0
400.0
phi1

FIGURE 8

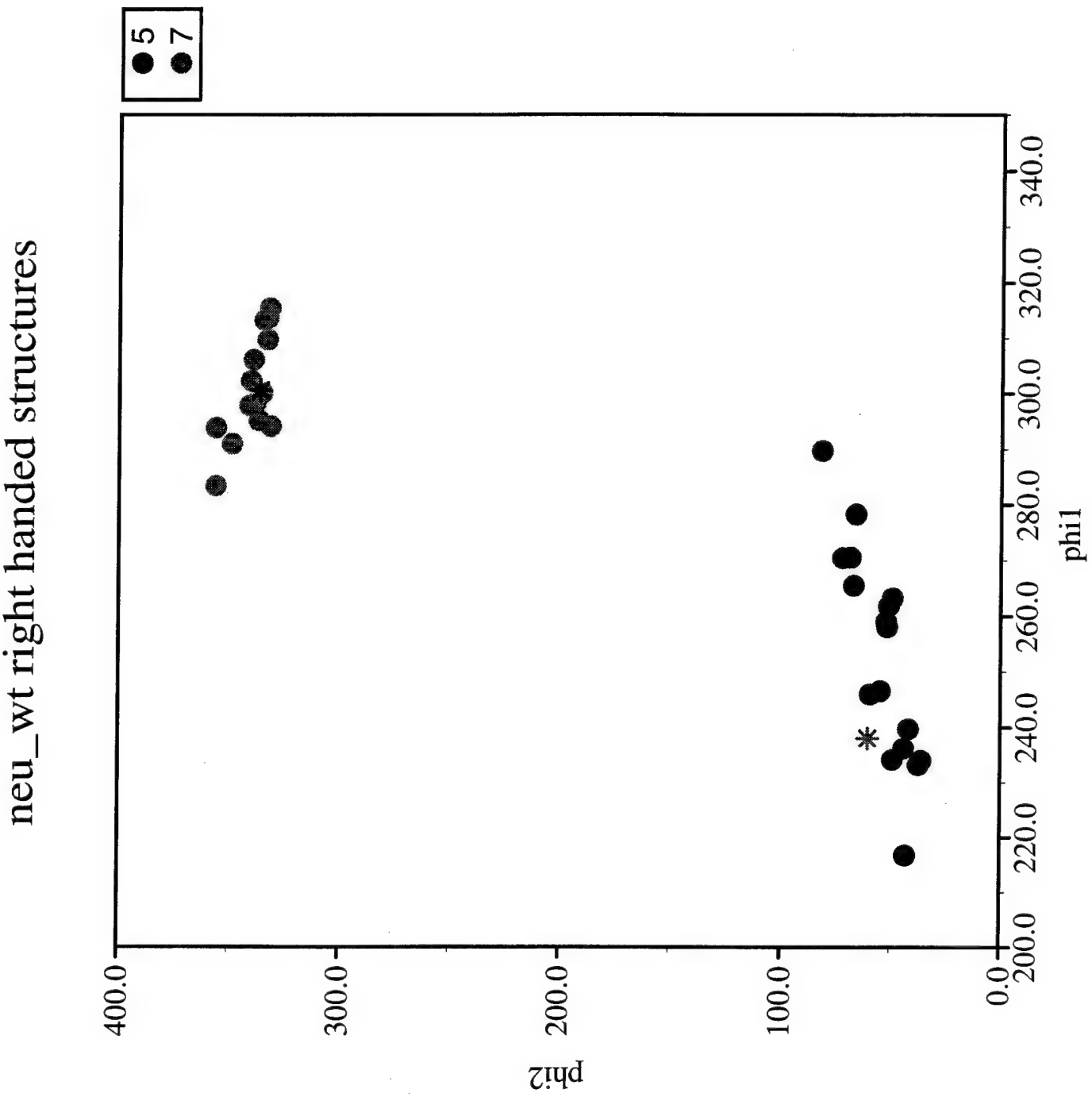
neu_wt right handed structures
5
7
400.0
300.0
200.0
100.0
0.0
phi2
200.0
220.0
240.0
260.0
280.0
300.0
320.0
340.0
phi1

FIGURE 9

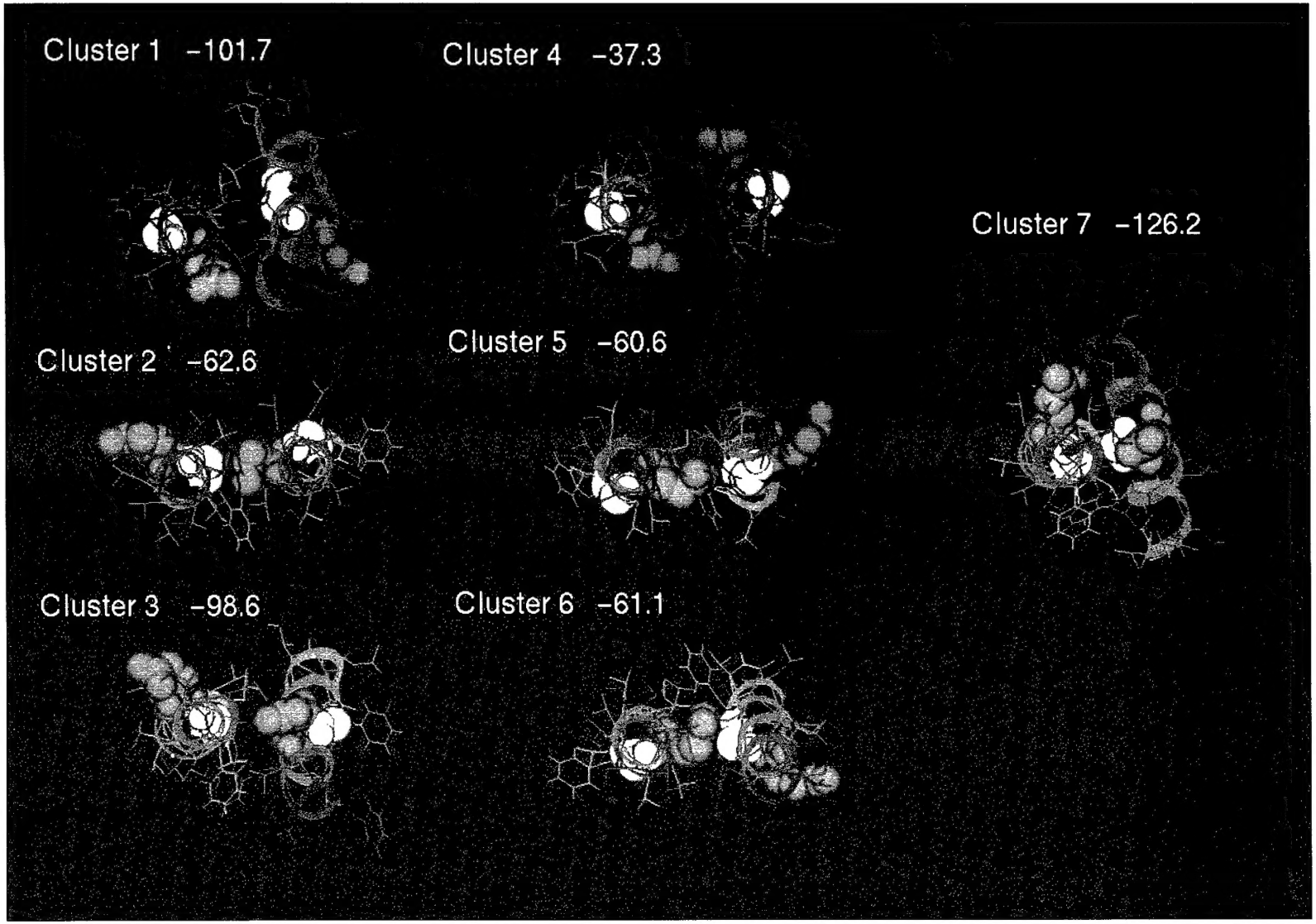
Cluster 1 -101.7
Cluster 4 -37.3
Cluster 7 -126.2
Cluster 2 -62.6
Cluster 5 -60.6
Cluster 3 -98.6
Cluster 6 -61.1

FIGURE 10

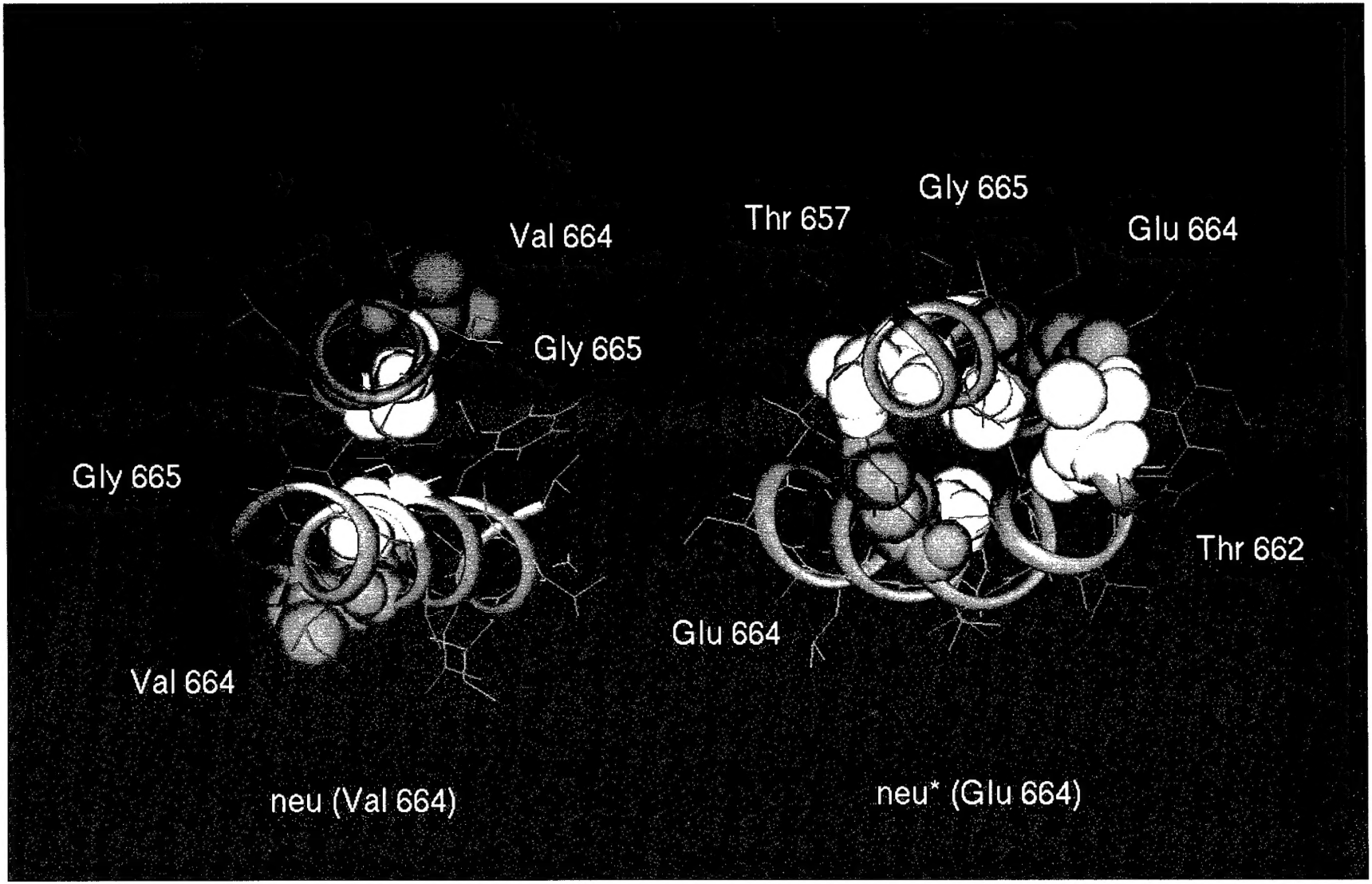
Val 664
Gly 665
Gly 665
Val 664
neu (Val 664)
Thr 657
Gly 665
Glu 664
Thr 662
Glu 664
neu* (Glu 664)

FIGURE 11

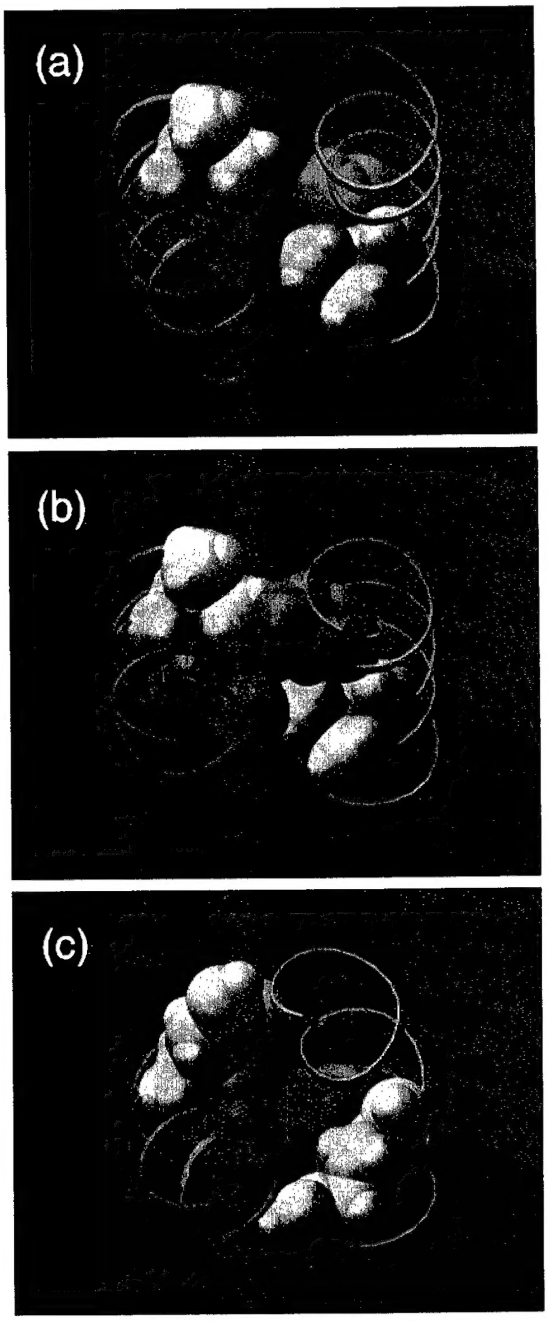


FIGURE 12

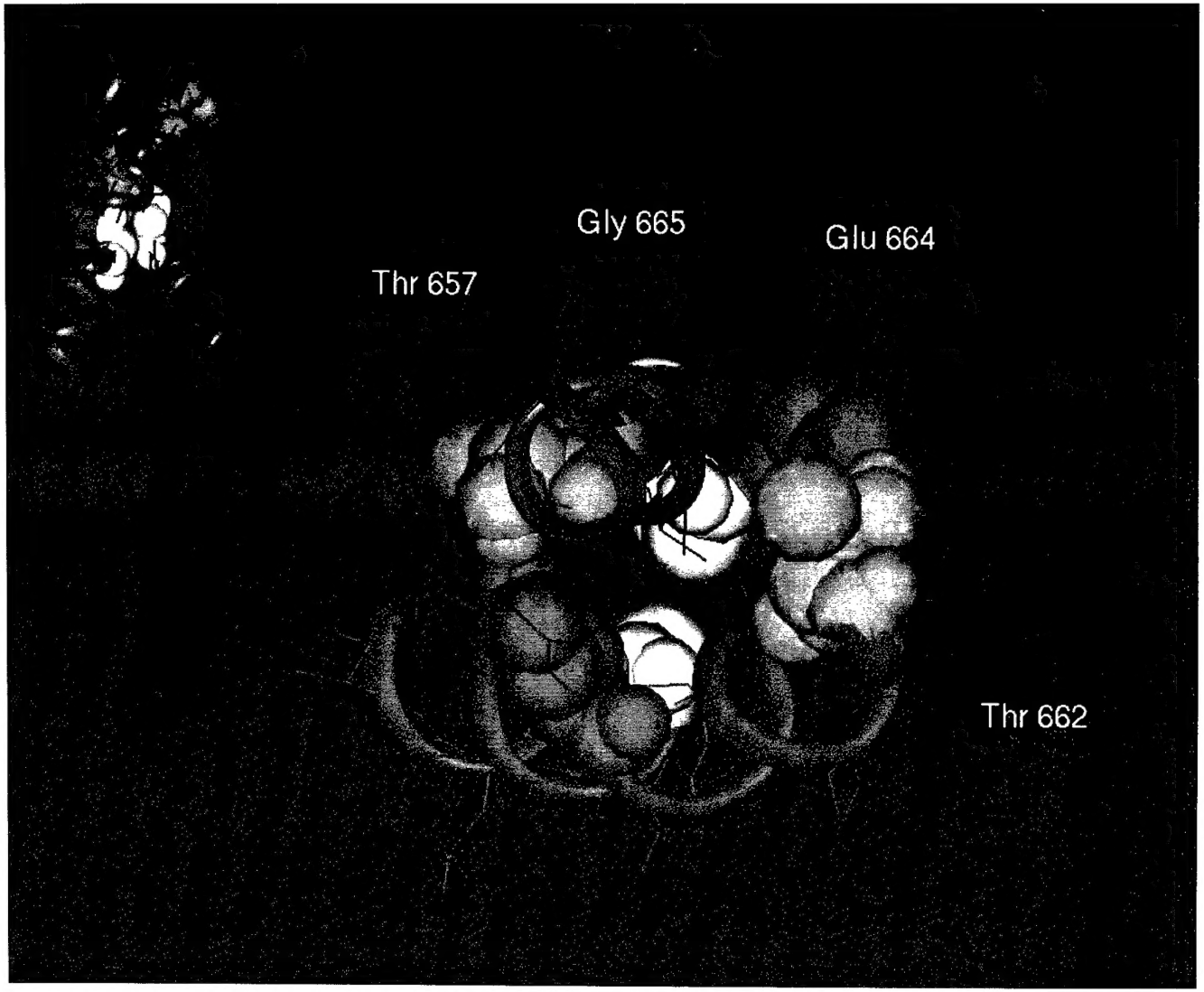


FIGURE 13